SUPPLEMENTARY INFORMATION

Hydrodynamics of a carbon nanotube

For rod-like structures, such as nanotubes, the viscous drag is described by an anisotropic hydrodynamic mobility tensor Γ_{ij} [1]. In the internal frame of a rigid body, this is diagonal and its components can be expressed as $\Gamma_{11} = \Gamma_{22} = \Gamma_\perp$ and $\Gamma_{33} = \Gamma_\parallel$, where $\Gamma_\perp$, $\Gamma_\parallel$ refer respectively to the translational mobility, transverse and parallel to the main axis [2]. For an axisymmetric object, the rotational mobility is expressed by only one coefficient, Γ_Θ. All coefficients depend on the length-to-diameter ratio $p = L/d$ as [2, 3]:

$$\Gamma_\perp = \frac{\ln p + \delta_\perp}{4\pi\eta L} \quad (1)$$

$$\Gamma_\parallel = \frac{\ln p + \delta_\parallel}{2\pi\eta L} \quad (2)$$

$$\Gamma_\Theta = \frac{3(\ln p + \delta_\theta)}{\pi\eta L^3} \quad (3)$$

where η is the water dynamical viscosity and δ_i are end-effect corrections calculated by Ref. [3] as polynomial expression of $\nu = (\ln 2p)^{-1}$:

$$\delta_\perp = 0.866 - 0.15\nu - 8.1\nu^2 + 18\nu^3 - 9\nu^4, \quad (4)$$

$$\delta_\parallel = -0.114 - 0.15\nu - 13.5\nu^2 + 37\nu^3 - 22\nu^4, \quad (5)$$

$$\delta_\Theta = -0.446 - 0.2\nu - 16\nu^2 + 63\nu^3 - 62\nu^4. \quad (6)$$

These are valid for $\nu < 0.45$, or $p > 4.6$ [3]. In our case, $d = 11$ nm, $L = 3\,\mu$m and $p = 273$, so we are well within the applicability of the theory. Note that the leading terms in Eqs4-6 differ from those in Ref.[3] because we add the end-effect correction to $\ln p$ instead of subtracting it from $\ln 2p$ [2].

Torque and Langevin equations

A single-beam optical trap is well approximated by an harmonic potential $V(x_i) = \frac{1}{2}\sum_{i=x,y,z} k_i x_i^2$ with spring constants $k_z < k_x, k_y$ [4]. The motion of a nanotube bundle can be described through the Euler angles ϕ, θ, ψ [5]. For an axisymmetric object, one can always choose $\psi = 0$, so that the corresponding rotation matrix from the laboratory coordinates x_i to the internal coordinates

(aligned with the principal inertia axes of the object) $x'_i = \mathcal{R}_{ij}(\phi,\theta)\, x_i$ is [5]:

$$\mathcal{R}(\phi,\theta) = \begin{pmatrix} \cos\phi & \sin\phi & 0 \\ -\cos\theta\sin\phi & \cos\theta\cos\phi & \sin\theta \\ \sin\theta\sin\phi & -\sin\theta\cos\phi & \cos\theta \end{pmatrix} \tag{7}$$

The torque exerted by the optical harmonic potential on the tilted SWNT bundle is the sum of the center of mass and inner torques. The center of mass coordinates, X_i, are uncorrelated stochastic variables. Thus, the time average of crossed terms of the type $X_i X_j$ can be neglected, so that they do not give a contribution in the correlation functions (see below) and in the Brownian dynamics [6]. Hence, the only relevant contributions to the angular fluctuations are given by the inner torque components $M_i(\phi,\theta)$. These can be calculated by integrating over the bundle mass density distribution $\rho(x'_i)$:

$$\begin{aligned} M_i(\phi,\theta) &= -\int d^3x' \frac{\rho(x'_i)}{m} \epsilon_{ijl} x_j k_l x_l \\ &= -\int d^3x' \frac{\rho(x'_i)}{m} \epsilon_{ijl} \left[\mathcal{R}^{-1}(\phi,\theta)\vec{x}'\right]_j k_l \left[\mathcal{R}^{-1}(\phi,\theta)\vec{x}'\right]_l \end{aligned} \tag{8}$$

where k_i are the spring constants of the trapping potential,ϵ_{ijl} is the Levi-Civita symbol [5], and m is the mass of the trapped object. Thus, we can write the torque components using the moments of inertia of the axisymmetric object $I_\perp = \int d^3x' \rho(x'_i)\,[x'^2 + z'^2]$ and $I_\parallel = \int d^3x' \rho(x'_i)\,[x'^2 + y'^2]$ (referred to rotation perpendicular and parallel to the main axis), as:

$$M_x = -(k_y - k_z)\frac{I_\perp - I_\parallel}{m} \sin\theta\cos\theta\cos\phi \tag{9}$$

$$M_y = -(k_x - k_z)\frac{I_\perp - I_\parallel}{m} \sin\theta\cos\theta\sin\phi \tag{10}$$

$$M_z = (k_y - k_x)\frac{I_\perp - I_\parallel}{m} \sin^2\theta\sin\phi\cos\phi \tag{11}$$

In the limit of small polar angle, $\theta \ll 1$, the component M_z responsible for rotation (precession) about the optical axis can be neglected. Also, for objects having length L much bigger than the diameter d, $L \gg d$, as for our long SWNT bundles, we can neglect the moment of inertia parallel to the main axis $I_\parallel (\propto d^2) \ll I_\perp (\propto L^2)$. Thus, using the projections on the lab axes $\Theta_x = \theta\sin\phi$ and $\Theta_y = \theta\cos\phi$, the torque on the trapped bundle is:

$$M_x \approx -(k_y - k_z)\frac{I_\perp}{m}\Theta_y = -k_{\Theta_y}\Theta_y \tag{12}$$

$$M_y \approx -(k_x - k_z)\frac{I_\perp}{m}\Theta_x = -k_{\Theta_x}\Theta_x \quad (13)$$

$$M_z \approx 0 \quad (14)$$

As expected, the xz (yz) motion is ruled by the M_y (M_x) torque component.

The Langevin equations [6] for centre-of-mass displacements $X_i(t)$ and angles $\Theta_j(t)$ in the lab frame can now be calculated. The trapping radiation force and viscous Stokes drag (i.e., the friction force exerted by the fluid on the fluctuating particle) are involved in the centre-of-mass displacement equations, while the radiation and viscous Stokes torque are responsible for counteracting the angular fluctuations:

$$\begin{aligned}
\partial_t X(t) &= -\Gamma_\perp k_x X(t) + \xi_x(t) \\
\partial_t Y(t) &= -\Gamma_\perp k_y Y(t) + \xi_y(t) \\
\partial_t Z(t) &= -\Gamma_\parallel k_z Z(t) + \xi_z(t) \\
\partial_t \Theta_x(t) &= -\Gamma_\Theta k_{\Theta_x} \Theta_x(t) + \xi_{\Theta_x}(t) \\
\partial_t \Theta_y(t) &= -\Gamma_\Theta k_{\Theta_y} \Theta_y(t) + \xi_{\Theta_y}(t)
\end{aligned} \quad (15)$$

where $\xi_i(t)$ are random noise sources with zero mean and variance $\langle \xi_i(t)\xi_i(t+\tau)\rangle = 2k_BT\Gamma_i\delta(\tau)$ (with $\delta(\tau)$ Dirac's δ-function). These equations lead to first order differential equations for the corresponding autocorrelation functions $C_{X_iX_i}(\tau) = \langle X_i(t)X_i(t+\tau)\rangle$ and $C_{\Theta_j\Theta_j}(\tau) = \langle \Theta_j(t)\Theta_j(t+\tau)\rangle$, e.g. for the $X(t)$ variable the corresponding autocorrelation function has to obey:

$$\partial_\tau C_{XX}(\tau) = -\Gamma_\perp k_x C_{XX}(\tau) \quad (16)$$

that is easily solved yielding the typical exponential decay [7]:

$$C_{XX}(\tau) = \frac{k_BT}{k_x} e^{-\Gamma_\perp k_x|\tau|} \quad (17)$$

Thus, the corresponding autocorrelation functions for the five stochastic variables $X, Y, Z, \Theta_x, \Theta_y$ decay with relaxation frequencies:

$$\begin{aligned}
\omega_x = \Gamma_\perp k_x,\ \omega_y = \Gamma_\perp k_y,\ \omega_z = \Gamma_\parallel k_z \\
\Omega_x = \Gamma_\Theta k_{\Theta_x},\ \Omega_y = \Gamma_\Theta k_{\Theta_y}.
\end{aligned} \quad (18)$$

From this model we can also calculate a parameter encompassing the hydrodynamics of SWNT bundles in the confined potential:

$$\frac{\Omega_i}{\omega_i} = \frac{\Gamma_\Theta k_{\Theta_i}}{\Gamma_\perp k_i} \quad (19)$$

For our sample, we have $L \approx 3$ μm and $d \approx 11$ nm ($p = 273$), and we can approximate the moment of inertia of the bundle with that of a rod $I_\perp = mL^2/12$. Thus, from Eqs. 1,3,12:

$$\frac{\Omega_i}{\omega_i} = \frac{\ln p + \delta_\Theta}{\ln p + \delta_\perp} \cdot \frac{k_i - k_z}{k_i}. \tag{20}$$

As an example, we can calculate Ω_i/ω_i for the data obtained at maximum power in Fig.4a,b of the main text, where $k_x = 23.9$ pN/μm, $k_y = 52.2$ pN/μm and $k_z = 0.72$ pN/μm. This gives $\Omega_i/\omega_i \approx 0.76$ for both axes. This can be compared with the ratio of the measured relaxation frequencies $\Omega_x = 0.9 \times 10^3 \mathrm{s}^{-1}$, $\omega_x = 4.4 \times 10^3 \mathrm{s}^{-1}$, $\Omega_y = 1.1 \times 10^3 \mathrm{s}^{-1}$, $\omega_y = 9.6 \times 10^3 \mathrm{s}^{-1}$, so that $\Omega_x/\omega_x \approx 0.2$ and $\Omega_y/\omega_y \approx 0.12$, i.e. 4 and 6 times smaller than above. Hence, in our experiments, the measured angular frequencies $\Omega_{x,y}$ are smaller than expected from a simple rod-like model. This reduction in rotational mobility can be accounted by considering the effect of radiation pressure. This can play a role by shifting the center of mass along z[8], and changing the pivot point for angular fluctuations. As a consequence, a decrease of rotational mobility is expected, due to its $1/L^3$ dependence (Eq. 3).

Correlation function of the Quadrant PhotoDiode signals

In back focal plane (BFP) interferometry, the interference pattern between forward scattered and un-scattered light in the microscope condenser BFP is imaged onto a four quadrant photodiode (QPD). For a spherical Mie scatterer, Pralle et al. [9] derived a three-dimensional model describing the QPD signals arising from this interference. When the lateral (X,Y) and axial (Z) displacements of the particle are small compared to the focal waist (of the order of 0.4μm) and Rayleigh length (of the order of 0.7μm) of the trapping laser beam, the resulting QPD signals are proportional to the bead displacements, the system works in a linear regime and the cross-talk within the signals is kept below an acceptable value of 10%. Although for an optically trapped nanotube a complete modeling is still missing, we expect a linear response with small cross-talk to be controlled by the same focal waist and Rayleigh range parameters as for a spherical scatterer. In our experiments (see Fig. 2 of the main text) displacements are within this range and, thus, we work in a linear response regime.

On the other hand, for a SWNT bundle the BFP interference pattern can change in two cases: a) the bundle is aligned with the optical axis, and the

interference changes because of center of mass displacements (X,Y,Z). Thus, in the linear regime, the QPD signals are proportional to these displacements; b) the SWNT bundle is tilted by a small angle θ, so that the change in BFP interference and QPD signals are proportional (to first approximation) to the projections of the nanotube on the lab frame axes. Thus, in the limit of small polar angle, $\theta \ll 1$, and under the assumptions discussed above, the QPD signals can be expressed in the lab frame as a superposition of the center of mass displacements and angular tilting of the SWNT bundle:

$$S_x \sim \beta_x \left(X + L\,\Theta_x\right);\; S_y \sim \beta_y \left(Y + L\,\Theta_y\right);\; S_z \sim \beta_z Z \tag{21}$$

where X,Y,Z are the center-of-mass coordinates, L is the bundle length, $L\Theta_x = L\theta \sin\phi, L\Theta_y = L\theta\cos\phi$ are its projections on the x and y axis. β_i are calibration factors that convert the QPD signals in displacements. They can be obtained from the autocorrelation functions amplitude after evaluation of the spring constants by using the equipartition theorem: $\beta_i = k_i C_{ii}(0)/k_B T$. From the data in Fig. 3 of the main text, we measure $\beta_x \approx 0.33V/\mu m$, $\beta_y \approx 0.4V/\mu m$, $\beta_z \approx 0.44V/\mu m$. These calibration factors enable the conversion from V to nm for the Brownian motion plots shown in Fig. 2.

The center-of-mass X_i and angular Θ_j coordinates are stochastic variables. The related autocorrelation functions $C_{ii}(\tau) = \langle S_i(t) S_i(t+\tau)\rangle$ are:

$$C_{xx} = \beta_x^2 \left[\langle X(t)X(t+\tau)\rangle + L^2 \langle \Theta_x(t)\Theta_x(t+\tau)\rangle\right] \tag{22}$$
$$C_{yy} = \beta_y^2 \left[\langle Y(t)Y(t+\tau)\rangle + L^2 \langle \Theta_y(t)\Theta_y(t+\tau)\rangle\right] \tag{23}$$
$$C_{zz} = \beta_z^2 \langle Z(t)Z(t+\tau)\rangle \tag{24}$$

where we assume center-of-mass and angular fluctuations to be uncorrelated, so that we can neglect cross terms of type $\langle X(t)\Theta_x(t+\tau)\rangle$. The autocorrelations of the transverse signals now contain combined information on center-of-mass and angular fluctuations and decay with lag time τ as a double-exponential with separated positional and angular relaxation frequencies.

Furthermore, the angular variables are correlated by the geometric relation $\Theta_x = \Theta_y \tan\phi$ and the cross-correlation of the transverse signals $C_{xy}(\tau) = \langle S_x(t) S_y(t+\tau)\rangle = C_{yx}(-\tau)$ is:

$$C_{xy} = \beta_x \beta_y L^2 \langle \Theta_x(t)\Theta_y(t+\tau)\rangle \tag{25}$$

To determine the evolution of C_{xy} we use the Langevin equations (Eqs. 15):

$$\begin{aligned}
\partial_\tau C_{xy} &= \beta_x\beta_y L^2 \langle \Theta_x(t)\partial_\tau \Theta_y(t+\tau)\rangle \\
&= -\beta_x\beta_y L^2\, \Omega_{\Theta_y} C_{xy} \qquad\qquad \tau > 0 \\
\partial_\tau C_{xy} &= \beta_x\beta_y L^2 \langle \Theta_x(t-\tau)\partial_\tau \Theta_y(t)\rangle \\
&= \beta_x\beta_y L^2\, \Omega_{\Theta_x} C_{xy} \qquad\qquad \tau < 0
\end{aligned} \tag{26}$$

and the solution can be summarized as:

$$C_{xy}(\tau) = \begin{cases} C_{xy}(0)\cdot e^{-\Omega_{\Theta_y}\tau} & \tau > 0 \\ C_{xy}(0)\cdot e^{-\Omega_{\Theta_x}\tau} & \tau < 0 \end{cases} \tag{27}$$

Thus, the cross-correlations decay as single exponentials with relaxation rates different for positive and negative lag times, corresponding to Ω_y and Ω_x.

As discussed above, we obtain the QPD signals assuming displacements within the linear response of the system and with small cross-talk between them. Using Eqs.22-24 we are able to fit well our experimental data (see Fig. 3 in the main text) with two exponential decays, and we can verify that the SWNT bundle displacements (see Fig. 2 in the main text) in the trap are well within this linear response regime. We now give an estimate of the small cross-talk occurring within the lateral S_x, S_y signals. Due to cross-talk we expect e.g. $S_x \propto X + \alpha Y + L\Theta_x$, with a related auto-correlation function $C_{xx} \propto \langle X(t)X(t+\tau)\rangle + \alpha^2\langle Y(t)Y(t+\tau)\rangle + L^2\langle \Theta_x(t)\Theta_x(t+\tau)\rangle$ composed of three exponential decays. By using the data in Fig. 3 of the main text, we have fit $C_{xx}(\tau)$ and $C_{yy}(\tau)$ with three exponential decays with relaxation frequencies $\omega_x, \omega_y, \Omega_x, \Omega_y$ fixed to those obtained in a two exponential decay fit, but keeping the amplitudes free. We get that lateral cross-talk is affects the auto-correlation function of about 1% and 0.3% for C_{xx} and C_{yy}, respectively. This ensures that the calibration for X and Y used in Fig. 2a have a cross-talk less than 10% and 5%, respectively.

Online movie

A movie is available showing how a bundle is trapped and aligned. Figure 1 below is a sequence of frames. When the laser is on, the bundle is trapped in the focal region of the laser(Fig.1a). The bundle is oriented along

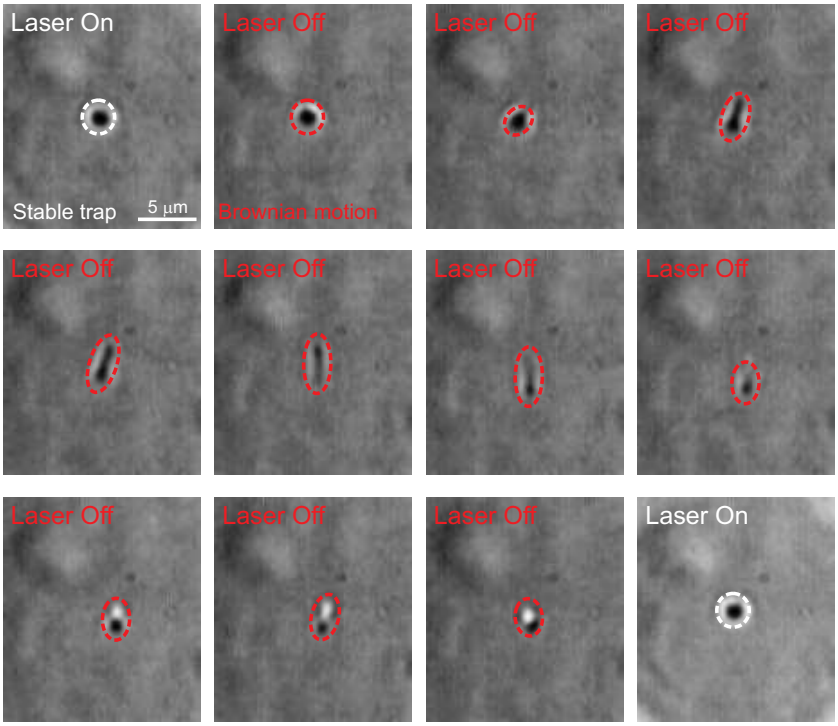

Figure 1: **Sequence of frames**. When the laser is on (**a**), the bundle is trapped and oriented in the focal region of the beam. When is off (**b-m**), the bundle is not trapped and fluctuates in both position and orientation. Finally, the laser is on again (**n**) and the bundle is trapped and aligned once more. The images on the CCD result from the diffraction and interference of light from the bundle. The darker, sharper parts of the imaged bundle are in focus, while the whiter,wider ones are away from the focal region.

the optical (z-)axis, i.e. the imaging axis. The resolution is above the diffraction limit. The transverse size results from integration of the scattered light on the CCD camera. When the bundle is trapped, its Brownian fluctuations occur on a spatial range smaller than the image resolution, at a rate faster than the acquisition frame rate. Instead, when the laser is off (Figs.1b-m), the bundle is not trapped and changes its dynamical configuration on all time scales. Thus, each image from Fig.1b to 1m is a snapshot of random displacements resulting from free Brownian motion. Finally, the laser is turned on again (Fig.1n) and the bundle is trapped and aligned again.

References

[1] Happel, J. & Brenner, H. *Low Reynolds Number Hydrodynamics*, Springer, Berlin, (1981).

[2] Tirado, M.M., Lopez Matinez, C., Garcia de la Torre, J. Comparison of theories for the translational and rotational diffusion coefficients of rod-like macromolecules. Application to short DNA fragments. *J. Chem. Phys.* **81**, 2047-2052 (1984).

[3] Broersma, S. Viscous force and torque constants for a cylinder. *J. Chem. Phys.* **74**, 6989 (1981).

[4] Borghese, F., Denti, P., Saija, R. & Iatí, M.A. Optical trapping of non-spherical particles in the T-matrix formalism. *Optics Express* **15**, 11984-11998 (2007).

[5] Goldstein, H., Poole, C.P., Safko, J.L. *Classical Mechanics*, 3rd ed. (Addison Wesley, 2001).

[6] Coffey, W.T., Kalmykov, Y.P., Waldron, J.T. *The Langevin Equation*, 2nd ed. (World Scientific, Singapore, 2004).

[7] Volpe, G. & Petrov, D. Torque detection using brownian fluctuations. *Phys. Rev. Lett.* **97**, 210603 (2006).

[8] Pauzauskie, P.J. *et al.* Optical trapping and integration of semiconductor nanowire assemblies in water. *Nature Mat.* **5**, 97-111 (2006).

[9] Pralle, A. *et al.* Three-Dimensional High-Resolution Particle Tracking for Optical Tweezers by Forward Scattered Light. *Microscopy Research and Tech.* **44**, 378-386 (1999).